Semiquantum Chaos in the Double-Well

Thomas C. Blum *
Physics Department, 510A
Brookhaven National Laboratory
Upton, NY 11973-5000, USA

Hans-Thomas Elze †
Institut für Theoretische Physik, Universität Regensburg
93053 Regensburg, Germany
Physics Department, University of Arizona
Tucson, AZ 85721, USA

February 5, 2008

Abstract

The new phenomenon of semiquantum chaos is analyzed in a classically regular double-well oscillator model. Here it arises from a doubling of the number of effectively classical degrees of freedom, which are nonlinearly coupled in a Gaussian variational approximation (TDHF) to full quantum mechanics. The resulting first-order nondissipative autonomous flow system shows energy dependent transitions between regular behavior and semiquantum chaos, which we monitor by Poincaré sections and a suitable frequency correlation function related to the density matrix. We discuss the general importance of this new form of deterministic chaos and point out the necessity to study open (dissipative) quantum systems, in order to observe it experimentally.

*E-mail: tblum@wind.phy.bnl.gov
†E-mail: elze@cernvm.cern.ch, hans-thomas.elze@physik.uni-regensburg.de

PACS numbers: 05.45, 03.65, 03.65.S, 03.65.G, 85.30.V

TPR-95-28
nlin-sys/9511007

1 Introduction

Recently the concept of semiquantum chaos has been introduced in order to characterize a particular form of deterministic chaos [1]. Namely, dynamical systems with both quantum and classical degrees of freedom may show irregular behavior due to their generic coupled nonlinearities [2, 3, 4]. The appearance of both quantum and classical degrees of freedom (d.o.f.) generally can be thought of as a more or less valid approximation, depending on the physical circumstances, describing a truly complex nondissipative quantum system.

For example, the authors of Ref. [2] considered the zero momentum (long wavelength) part of the problem of pair production of charged scalar particles by a strong external electric field. In this limit the problem could be reduced to a classical oscillator interacting with a quantum mechanical one through a biquadratic coupling; i.e. a two d.o.f. system, one classical and the other purely quantum. They represent the electromagnetic vector potential and the charged matter field, respectively. In this case and for a physically motivated subset of all possible initial conditions, the dynamics can be mapped onto an equivalent completely classical problem with two effective d.o.f. Their motion is described by two coupled nonlinear second-order differential equations, which yield regular or irregular trajectories depending on initial conditions and suitably chosen model parameters. Clearly, an approximation to a purely quantum system, a quantum field theory in fact, has been treated here and eventually gives rise to deterministic chaos in an equivalent low-dimensional classical system.

The latter observation presents the starting point of our investigation of semiquantum chaos in the one-dimensional double-well problem. It can be considered as the zero-dimensional limit of the scalar Higgs field model [5]. To study the entropy production and thermalization in strong interactions at ultrarelativistic energies a related scalar quantum field theory has recently been treated in the time-dependent Hartree-Fock approximation (TDHF) equivalent to a Gaussian variational principle [6, 7] (see also further references therein). The resulting field equations in the long wavelength limit, i.e. neglecting spatial variations, reduce to a coupled pair of Hartree-Fock type equations for one-dimensional double-well oscillators. They represent a semiclassical approximation to the full quantum problem in terms of spatially homogenous fast and slow modes, respectively. The equations for a single

such oscillator will be given in Section II and their solutions studied in detail in the following.

At this point it seems sufficient to state that mean-field type TDHF quantum corrections to the classical equation for the double-well oscillator, which behaves regularly in the classical limit, introduce characteristic nonlinear features including additional effectively classical d.o.f. They, however, describe quantum fluctuations of the basic coordinates and conjugate momenta. Such additional d.o.f. are an essential element to allow for the possibility of semiquantum chaos. We recall that a classical one-dimensional anharmonic oscillator, which can be described by a set of two autonomous first-order differential equations, cannot have chaotic trajectories according to the Poincaré-Bendixson theorem [1], which rules out chaotic flow in a bounded region in two-dimensional (phase) space.

The time-dependent variational principle [7] using generalized Gaussian trial wave functions has, in fact, already been applied in quantum chemistry for quite a while (see Refs. [8, 9] for some early and more recent work, respectively, citing numerous further relevant references). However, it has only recently been pointed out that the parameters (parameter functions in field theory [6]) specifying the Gaussian wave functions (functionals in field theory) are governed by a set of equations according to the variational principle which describe an equivalent classical Hamiltonian system [3]. It is this equivalent classical system which may show what has been termed semiquantum chaos, even if the subset of equations belonging to the proper classical limit (neglecting quantum fluctuation d.o.f.) produces only strictly regular motion. Furthermore, it is generally believed that the full quantum dynamics obeying the Schrödinger wave equation, which is a linear partial differential equation (however, a functional l.p.d. equation in field theory), is always regular (see Refs. [3, 9] for further discussions on this point). Thus, the question of quantum chaos usually pertains to more subtle aspects of the dynamics which reflect some traces of deterministic chaos in the corresponding classical system [1, 9], if at all.

Presently, we want to address the question instead, rather independently of the behavior of the full quantum dynamics or even a regular classical limit thereof, whether or how the onset of semiquantum chaos is related to the breakdown of the underlying semiclassical approximation. Correspondingly, one may reconsider the often posed problem of whether or where in the relevant classical phase space there are regions in which the system can safely

be or even has to be studied using a semiclassical approach [10].

Finally, we want to draw attention to Ref. [4]. There, the possibility of chaotic behavior without classical counterpart is pointed out in a many-body system undergoing multiple resonant tunneling. More specifically, an electron cloud in a three-well heterostructure was represented by an effective one-particle wave function obeying a nonlinear Hartree equation. Clearly, the inherently semiclassical description gives rise to the essential nonlinearity of the second-order partial differential equation again. However, the authors of this work speculate that the many-body character of the system, i.e. infinitely many d.o.f. already on the classical field level, might stabilize the reported semiquantum chaos in this case to persist even in a fully quantum treatment. This necessitates a time-dependent approach to quantum field theory, which has not been worked out for the nonrelativistic problem at hand to date. We will come back to this in the final section where we discuss one possible first step beyond our present simple double-well oscillator model in the direction of a quantum field theory, which is motivated by the above mentioned issues [4, 6]. In any case, it is gratifying that at least for solid state heterostructures an experimental verification of semiquantum chaos seems within reach (see further references in [4].

Our paper is organized as follows. Section II defines the model and describes briefly the time-dependent variational principle, from which we obtain our basic set of equations. In Section III we present some analytical considerations and introduce the effective semiquantum potential, which should help to visualize the results of our numerical studies presented in Section IV. In Section V we briefly compare the semiquantum dynamics with exact solutions of the Schrödinger equation and summarize our results. We point out some interesting problems related to environment-induced decoherence and chaotic entropy production in open quantum systems, which are left for future work.

We discuss qualitatively there, how semiquantum chaos can be reconciled with a regular classical limit and the intrinsic linearity of quantum mechanics, in particular.

2 The Semiclassical Double-Well Oscillator

The purpose of this section is to introduce our toy model of the simple one-dimensional double-well oscillator which, however, will be studied in a non-perturbative semiclassical approximation (TDHF, cf. below). As explained in the Introduction, we consider this as a necessary first step towards the study of a (3+1)-dimensional field theory [6]. The classical action of our model is given by

$$S = \int dt \, \{\frac{1}{2}(\partial_t \varphi)^2 - v(\varphi)\} \ , \tag{1}$$

with

$$v(\varphi) \equiv -\frac{1}{2}\mu^2\varphi^2 + \frac{\lambda}{4!}\varphi^4 \ , \tag{2}$$

and $\varphi \equiv \varphi(t)$ denotes the oscillator coordinate, which is the analogue of a scalar field, $\varphi \equiv \varphi(x,t)$, in zero space dimensions. Note that the potential includes a negative "mass" term $\sim \mu^2$, which allows for spontaneous symmetry breaking in the anharmonic potential $\sim \varphi^4$. Fig. 1 shows the potential $v(\varphi)$ for the typical model parameters used throughout this work, $\mu^2 = 1.0, \lambda = 0.06$ (we employ units such that $\hbar = c = 1$) together with a typical classical phase space trajectory oscillating in one of the wells.

The Schrödinger equation following from eq. (1) (coordinate representation),

$$i\partial_t \psi(\varphi;t) = \hat{H}\psi(\varphi;t) = \{-\frac{1}{2}\frac{d^2}{d\varphi^2} + v(\varphi)\}\psi(\varphi;t) \ , \tag{3}$$

is linear in the wave function ψ. Thus, there is no mixing of its Fourier components,

$$\psi(\varphi;\omega) \equiv \int_{-\infty}^{\infty} dt \ \mathrm{e}^{-i\omega t}\psi(\varphi;t) \ , \tag{4}$$

which allows a trivial decomposition of the full quantum dynamics w.r.t. fast and slow modes. This explains why at first sight one does not expect quantum chaos, no matter whether the corresponding classical system behaves regularly or not, and why many efforts have been made to find traces of classical chaos in the fully quantized system (see, e.g., Refs. [1, 9, 11] and further references therein).

We remark here that the situation for the field theory functional Schrödinger equation, despite its apparent similarity to eq. (3), seems even more complex,

since the relation of the physical (most commonly employed single-particle) observables to the wave functional is more complicated in this case. This is exemplified already by the quantum Brownian motion of a single particle interacting with a quantized electromagnetic field, phonon, or other radiation field [6, 12, 13], cf. Section V.

Presently, we do not follow the established routes of investigations into quantum chaos. Rather, we study chaotic behavior generated in the semiclassical regime even for classically regular systems, such as our model defined by eqs. (1), (2). Before we derive the relevant equations of motion here, we pause to consider the observables of our model in more detail. Apart from the usual expectation values of the coordinate and its conjugate momentum,

$$\bar{\varphi}(t) \equiv \langle \hat{\varphi} \rangle \quad , \quad \bar{\pi}(t) \equiv \langle \hat{\pi} \rangle = \langle -i \frac{d}{d\varphi} \rangle \quad , \tag{5}$$

we will be particularly interested in expectation values of functions of φ,

$$O_{\varphi}(t) \equiv \langle O(\hat{\varphi}) \rangle = \int_{-\infty}^{\infty} d\varphi \; \psi(\varphi;t) O(\varphi) \psi^{*}(\varphi;t) \quad , \tag{6}$$

i.e. fluctuation variables. By Fourier transformation we obtain

$$O_{\varphi}(\omega) = \int_{-\infty}^{\infty} d\varphi \int_{-\infty}^{\infty} \frac{d\omega'}{2\pi} \; \psi(\varphi;\omega') O(\varphi) \psi^{*}(\varphi;\omega'-\omega) \quad . \tag{7}$$

Thus, we have to find the spectrum of frequencies in

$$\rho(\varphi,\varphi;\omega) \equiv \int_{-\infty}^{\infty} \frac{d\omega'}{2\pi} \; \psi(\varphi;\omega') \psi^{*}(\varphi;\omega'-\omega) \quad , \tag{8}$$

which is the Fourier transform of a diagonal element of the density matrix which pertains to the pure state $|\psi(t)\rangle$ (coordinate representation). For simplicity we do not consider the off-diagonal density matrix elements at present, which would be needed to evaluate more general observables $\langle O(\hat{\varphi},\hat{\pi}) \rangle$. Clearly, the diagonal elements $\rho(\varphi,\varphi;\omega)$ yield a frequency correlation function defined at each point φ, which presents a simple and particularly useful example out of a large variety of higher order correlation functions.

In order to illustrate the information provided by the frequency correlation function, we evaluate it formally in the full quantum case. Using the fact that the spectrum of the double-well Schrödinger equation (3) corresponds to discrete stationary bound states,

$$\psi_n(\varphi;t) = \phi_n(\varphi)\mathrm{e}^{i\omega_n t} \quad , \tag{9}$$

gives

$$\psi_n^{(*)}(\varphi;\omega) = 2\pi\phi_n^{(*)}(\varphi)\delta(\omega-\omega_n) \quad . \tag{10}$$

A general pure state is

$$\psi(\varphi;\omega) = 2\pi\sum_n c_n\phi_n(\varphi)\delta(\omega-\omega_n) \quad . \tag{11}$$

Then, we obtain from eqs. (8) and (11)

$$\rho(\varphi,\varphi;\omega) = \sum_{n,n'} M_{nn'}(\varphi)\delta(\omega-\omega_n+\omega_n') \quad , \tag{12}$$

i.e. a spectrum of discrete lines arising at all $\omega = \omega_n - \omega_n'$, with a strength

$$M_{nn'}(\varphi) \equiv 2\pi c_n c_{n'}^* \phi_n(\varphi)\phi_{n'}^*(\varphi) = M_{n'n}^* \quad . \tag{13}$$

The strength matrix M is Hermitean and time-independent, implying constant real eigenvalues. In particular,

$$\begin{aligned} \rho(\varphi,\varphi;\omega=0) &= \mathrm{const}\cdot \mathrm{Tr}M(\varphi) = \int_{-\infty}^{-\infty} dt\ \psi(\varphi;t)\psi^*(\varphi;t) \\ &= \mathrm{const}\cdot 2\pi\sum_n |c_n|^2|\phi_n(\varphi)|^2 \quad . \end{aligned} \tag{14}$$

Thus, the strengths of the lines depend on the actual state under consideration, i.e. the amplitudes c_n, and are completely determined by the initial condition, $\psi(\varphi;t=0)$, whereas their positions are given by the distribution of the energy level spacings of the system. We will employ the frequency correlation function as a diagnostic tool in Section IV to monitor the onset of semiquantum chaos, in which case the frequency correlation function becomes increasingly noisy with its discrete line character eventually disappearing completely.

Next, we turn to the derivation of appropriate semiquantum equations of motion. The TDHF or Gaussian variational approximation can be easily obtained with the help of Dirac's variational principle [7]. The latter can be stated as follows:

$$\frac{\delta\Gamma[\psi]}{\delta\psi} = 0 \quad , \quad \text{for all } \psi \ \text{ with } \langle\psi|\psi\rangle = 1 \quad , \tag{15}$$

and

$$\Gamma[\psi] = \int dt \ \langle\psi(t)|(i\partial_t - \hat{H})|\psi(t)\rangle \quad , \tag{16}$$

i.e. requiring the effective action Γ defined in eq. (16) to be stationary against arbitrary variations of the normalized wave function, which vanish at $t \to \pm\infty$, is equivalent to the exact Schrödinger equation (3). With the variational principle one can solve the quantum mechanical time-evolution problem approximately by restricting the variation of the wave function to a subspace of the full Hilbert space.

In the following we work with properly normalized Gaussian trial wave functions,

$$\begin{aligned} \psi_G(\varphi;t) \ \equiv \ & (2\pi G(t))^{-\frac{1}{4}} \exp\{-[\frac{1}{4}G^{-1}(t) - i\sigma(t)][\varphi - \bar{\varphi}(t)]^2 \\ & + i\bar{\pi}(t)[\varphi - \bar{\varphi}(t)]\} \quad , \end{aligned} \tag{17}$$

which leads to the TDHF approximation via the evaluation of the effective action, eq. (16), i.e. by performing simple Gaussian integrations. Thus, we obtain:

$$\begin{aligned} \Gamma[\psi_G] \ = \ & \int dt \Big\{ \bar{\pi}\dot{\bar{\varphi}} - \frac{1}{2}\bar{\pi}^2 - v(\bar{\varphi}) \\ & + \hbar[\sigma\dot{G} - 2\sigma^2 G - \frac{1}{8}G^{-1} - \frac{1}{2!}v''(\bar{\varphi})G] - \frac{3}{4!}\hbar^2 v''''(\bar{\varphi})G^2 \Big\} \quad , \end{aligned} \tag{18}$$

with $v''(\bar{\varphi}) = -\mu^2 + \frac{1}{2}\lambda\bar{\varphi}^2$, $v''''(\bar{\varphi}) = \lambda$ from eq. (2). In eq. (18) we inserted the appropriate factors of $\hbar$ which exhibit the classical and semiquantum contributions to the effective action. Clearly, the dynamics is now described by the four time-dependent functions which parametrize the trial wave function, eq. (17). Here $\bar{\varphi}$ and G play the role of the effective coordinates, while $\bar{\pi}$ and σ present the conjugate momenta. This is further illustrated by the

expectation values,

$$\langle\varphi\rangle_G = \bar{\varphi}(t) \ , \quad \langle -i\frac{d}{d\varphi}\rangle_G = \bar{\pi}(t) \ , \tag{19}$$

and

$$\langle\varphi^2\rangle_G = \bar{\varphi}^2(t) + G(t) \ , \quad \langle i\partial_t\rangle = \bar{\pi}(t)\dot{\bar{\varphi}}(t) - \dot{\sigma}(t)G(t) \ , \tag{20}$$

which are calculated using eq. (17). Furthermore,

$$\begin{aligned} (\langle\varphi^2\rangle_G - \bar{\varphi}^2)^{\frac{1}{2}} \cdot (\langle\pi^2\rangle_G - \bar{\pi}^2)^{\frac{1}{2}} &= G^{\frac{1}{2}} \cdot (\frac{1}{4}G^{-1} + 4\sigma^2 G)^{\frac{1}{2}} \\ &= \frac{1}{2}(1 + (4\sigma G)^2)^{\frac{1}{2}} \geq \frac{1}{2} \ , \end{aligned} \tag{21}$$

which demonstrates the uncertainty relation in the present context. Minimum uncertainty coherent states yield the lower bound on the r.h.s. of eq. (21).

Finally, the semiquantum equations of motion are obtained as the Euler - Lagrange equations for the effective action, eq. (18), by independent variations w.r.t. $\bar{\varphi}$, $\bar{\pi}$, G and σ:

$$\dot{\bar{\varphi}} = \bar{\pi} \ , \tag{22}$$

$$\dot{\bar{\pi}} = -v'(\bar{\varphi}) - \frac{\hbar}{2}v'''(\bar{\varphi})G \ , \tag{23}$$

$$\dot{G} = 4\sigma G \ , \tag{24}$$

$$\dot{\sigma} = -2\sigma^2 + \frac{1}{8}G^{-2} - \frac{1}{2}v''(\bar{\varphi}) - \frac{\hbar}{4}v''''(\bar{\varphi})G \ , \tag{25}$$

with $v'(\bar{\varphi}) = -\mu^2\bar{\varphi} + \frac{\lambda}{3!}$, $v'''(\bar{\varphi}) = \lambda\bar{\varphi}$, and v'', v'''' as given after eq. (18). Several remarks are in order here:

- Equations (22)-(25) present a coupled set of four autonomous first-order nonlinear differential equations, which explains the potential for semiquantum chaos of the double-well oscillator, for example.

- Equivalently, by eliminating the momenta $\bar{\pi}$ and σ, one obtains two coupled second-order equations, which bear some characteristic resemblance to eqs. (16) in Ref. [2], i.e. the particle production problem mentioned in the Introduction.

- It follows from eq. (18) that only eqs. (22), (23) survive the simple-minded classical limit with $\hbar \to 0$; thus, eqs. (24), (25) present the dynamics of an additional effectively classical d. o. f., which arises through the semiclassical approximation of (Gaussian) quantum fluctuations.

The TDHF approximation in the form of eqs. (22) - (25) was previously studied for various quantum mechanical models in Ref. [14]; the potential for semiquantum chaos, however, has only recently been noticed based on a derivation via Ehrenfest's theorem [3]. Note that the above equations of motion decouple and can be solved analytically, of course, in the harmonic limit, $v'' = \text{const}$, $v''' = v'''' = 0$.

To conclude this section, note that the frequency correlation function, eq. (8), in TDHF approximation is given by

$$\rho(\varphi, \varphi; \omega) = \int_{-\infty}^{\infty} dt \; \mathrm{e}^{-i\omega t} (2\pi G)^{\frac{1}{2}} \exp\{-\frac{1}{2} G^{-1} [\varphi - \bar{\varphi}]^2\} \quad , \tag{26}$$

using eq. (17). Clearly, the magnitude of G determines the admissible amount of quantum fluctuation around the classical expectation value $\bar{\varphi}$, cf. (19), such that the integrand in eq. (26) is not negligible. Thus, the relevant contributions to $\rho(\varphi, \varphi; \omega)$ come from those parts of a semiquantum trajectory of the system, i.e. $\{\bar{\varphi(t)}, G(t)\}$, which are sufficiently close to the point φ and have a time dependence characterized approximately by the frequency ω.

3 Energy, Effective Potential and Instabilities

The purpose of this section is to report some analytical considerations, which may help to better understand the dynamics of the semiquantum equations of motion, eqs. (22) - (25).

To begin with, the Hamiltonian contribution to the effective action, cf. eqs. (16), (18) together with the second of eqs. (20), yields the conserved total energy for our nondissipative model. The resulting expression is still a rather complicated function of $\bar{\varphi}$, $\bar{\pi}$, G, and σ. For simplicity, we choose

initial conditions with zero momenta in the following, $\bar{\pi}(t=0) = \sigma(t=0) = 0$. Then, evaluating the total energy, E_0, at the minimum of the classical potential, for example, we obtain

$$E_0(G) = \frac{1}{8}G^{-1} - \frac{3}{2}\frac{\mu^4}{\lambda} + \mu^2 G + \frac{1}{8}\lambda G^2 \quad . \tag{27}$$

With all other parameters kept fixed, the initial energy or, equivalently, the initial value $G(t=0)$ is the relevant control parameter for our model.

Furthermore, comparing the initial value $E_0(G)$ with the total energy evaluated at any later time, we obtain a simple measure for the numerical accuracy of the simulations to be discussed in Section IV.

Secondly, in analogy to a classical system in two dimensions ("coordinates" $\bar{\varphi}$ and G), we consider the effective potential which is defined as the total minus the kinetic energy, i.e. $V(\bar{\varphi}, G) \equiv E(\bar{\varphi}, G; \bar{\pi} = \sigma = 0)$, in terms of the total energy. Thus,

$$V(\bar{\varphi}, G) = v(\bar{\varphi}) + \hbar[\frac{1}{8}G^{-1} + \frac{1}{2!}v''(\bar{\varphi})G] + \frac{3}{4!}\hbar^2 v''''(\bar{\varphi})G^2 \quad , \tag{28}$$

which shows the classical contribution plus quantum corrections. In Fig. 2 we present a contour plot of equipotential lines for the effective potential. Its most interesting feature is the valley in the potential energy surface which leads to a "saddle point region" (cf. below) separating the two effective potential wells. Thus, our semiclassical potential shares some similarity with the classical "demonic potential" studied in Ref. [9]. By analogy, we expect also in our case energy dependent transitions between regular and chaotic motion in the effective potential, which will be confirmed in the next section.

Clearly, by opening the possibility to move into the semiclassical G-direction, our system can roll around the hill at $\bar{\varphi} = G = 0$, i.e. around the equivalent of the classical local maximum of the potential at $\bar{\varphi} = 0$. This "roll around" represents the quantum mechanical tunneling through the given potential barrier in the semiclassical TDHF approximation. Note, however, that the limits $G \to 0$ and $\hbar \to 0$ do not commute in eq. (28) due to the singular term $\sim \hbar/G$, which makes the proper classical limit a nontrivial affair here as well as in the equations of motion, eqs. (22) - (25).

Next, we observe that there are five fixed points of the flow described by eqs. (22) - (25). They correspond to the three extrema of the classical potential and are determined in the semiquantum case by the conditions

$\dot{\bar{\varphi}} = \dot{\bar{\pi}} = \dot{G} = \dot{\sigma} = 0$. These, by the equations of motion together with eq. (28), become $\bar{\pi} = \sigma = \frac{\partial V}{\partial \bar{\varphi}} = \frac{\partial V}{\partial G} = 0$, in analogy to the classical case.

A first solution corresponding to the center of the saddle point region of the effective potential, cf. Fig. 2, is given by $\bar{\varphi} = 0$ and $G = f(\frac{2\mu^2}{3\lambda}, \frac{1}{4\lambda})$ with

$$f(a,b) \equiv a + (b + a^3 + [b^2 + 2ba^3]^{\frac{1}{2}})^{\frac{1}{3}} + (b + a^3 - [b^2 + 2ba^3]^{\frac{1}{2}})^{\frac{1}{3}} \quad .$$

For $\mu^2 = 1.0$, $\lambda = 0.06$ we find $G \approx 33.341$. However, this turns out to be a small dip in the potential energy surface, since there are two fixed points close by. They are given by

$$\bar{\varphi} = \pm(\frac{6\mu^2}{\lambda} - 3G)^{\frac{1}{2}} \quad , \quad \text{with} \;\; G = \frac{2\mu^2}{3\lambda}(1 + 2\cos\frac{\alpha}{3}) \quad , \quad \cos\alpha = 1 - (8\lambda(\frac{2\mu^2}{3\lambda})^3)^{-1} \quad .$$

For the above parameter values we find $\bar{\varphi} \approx \pm 0.106$, $G \approx 33.330$. Finally, the fixed points corresponding to the minima of the two deep effective potential wells are given by the previous formulae for $\bar{\varphi}$ and G, however, replacing $\alpha \to \alpha - \pi$ in the equation for $\cos\alpha$ only. Thus, we obtain here $\bar{\varphi} \approx \pm 9.947$, $G \approx 0.355$. Naturally, one may expect the trajectories to behave regularly, if they are initiated with sufficiently small momenta $(\bar{\pi}, \sigma)$ sufficiently close to the fixed points which correspond to (local) minima of the effective potential.

Furthermore, note that the number of fixed points has increased by two as compared to the classical limit. We conjecture that the number of fixed points would keep increasing, if we would include corrections of higher order in $\hbar$ into the effective action, eq. (18), and therewith into the equations of motion. Equivalently, one would have to go beyond the Gaussian ansatz for the wave function, eq. (17), which will be further discussed in Section V.

Finally, we turn to the investigation of instabilities arising in the equations of motion, which might signal the onset of chaotic behavior. It is well known that ordinary pertubation theory w.r.t. the nonlinear coupling, i.e. λ at present, would not give the irregular break-up of KAM tori etc. for our conservative dynamical system generated by the TDHF approximation [1, 11]. Therefore, we eliminate the momenta $(\bar{\pi}, \sigma)$ from eqs. (22) - (25) in order to rewrite them in second-order form and, thus, to expose the analogy to coupled (potentially unstable) oscillators. We obtain from eqs. (22), (23):

$$\ddot{\bar{\varphi}} + m_{eff}^2 \bar{\varphi} = 0 \quad , \tag{29}$$

with

$$m_{eff}^2 \equiv \frac{1}{3!}\lambda\bar{\varphi}^2 + \frac{1}{2}\lambda G - \mu^2 \quad . \tag{30}$$

From eqs. (24), (25) one finds:

$$\ddot{G} + M_{eff}^2 G = \frac{1}{2}\frac{\dot{G}^2 + 1}{G} \quad , \tag{31}$$

with

$$M_{eff}^2 \equiv \lambda\bar{\varphi}^2 + \lambda G - 2\mu^2 \quad . \tag{32}$$

Obviously, both oscillators can become unstable due to exponentially growing modes for a finite range of (initial) values for $\bar{\varphi}$ and σ. Both effective mass squared terms become negative for

$$0 < G < \frac{2\mu^2}{\lambda} - \bar{\varphi}^2 \quad . \tag{33}$$

Note that the repulsive term on the r.h.s. of eq. (31) keeps $G > 0$ at all times. Thus, there is a region in the positive $\bar{\varphi}$-G-halfplane, where we expect trajectories with slightly different initial conditions (keeping for simplicity $\bar{\pi} = \dot{\bar{\varphi}} = \sigma = \dot{G} = 0$ initially) to diverge exponentially.

However, eq. (33) seems to provide at best a criterion for the local sensitivity to initial conditions. In particular, for initial conditions corresponding to high energy, i.e. sufficiently small $G(t = 0)$ according to eq. (27), one may expect the trajectories to behave rather regularly, since the unstable region in the $\bar{\varphi}$-G-plane by eq. (33) becomes a smaller and smaller fraction of the accessible one with increasing energy. These effects will be seen in our numerical results to be presented in the following section.

4 Numerical Results

In this section we present the results of numerically studying the solutions of the semiquantum equations of motion, eqs. (22) - (25), for a variety of initial conditions. However, we always fixed $\bar{\pi} = \sigma = 0$ initially and chose $G = 0.1$ together with various values for $\bar{\varphi}$ to represent initial configurations with varying total energy, $E(\bar{\pi} = \sigma = 0) = V(\bar{\varphi}, G)$, cf. eq. (28). Generally, we did not explore the full set of all initial conditions at a given energy, which would require much more extensive numerical calculations.

To begin with, we show in Fig. 3 the results for two energies which are very close to the absolute minimum, $E_{min} \approx -24.2948$; E_{min} is obtained at

the minima of the effective potential ($\bar{\varphi} = \pm 9.947$, $G = 0.355$) discussed previously. Thus, we observe in the left column of Fig. 3, which pertains to the lowest energy, a rather simple regular motion characterized by the basic oscillator frequency $\omega_0 = \sqrt{2}$ and a second frequency at twice this value. Note that the value of ω_0 is obtained by expanding the classical potential, eq. (2), around one of its minima and identifying the coefficient of the harmonic term, i.e. $\frac{1}{2}\omega_0^2 = \mu^2 = 1.0$, at present. Together with the frequency correlation function, cf. eqs. (8), (12), and (17), we present two Poincaré sections in the phase space planes of the two conjugate pairs of variables, $\{\bar{\pi}, \bar{\varphi}\}$ and $\{\sigma, G\}$, respectively.

Furthermore, a full trajectory is portrayed in the last row in Fig. 3. Clearly, a slight increase of the energy, with the corresponding results presented in the second column here, immediately leads to the admixture of higher multiples of the basic frequency ω_0. In this case, the Poincaré sections still look fairly simple, but the picture of a trajectory already shows a rather convoluted structure. Obviously, the increasing complexity of trajectories can be expected to be reflected in the more and more detailed fine structure of the frequency correlation function as the energy is increased further.

Before we proceed, a few remarks are in order here concerning the numerical solution of the equations of motion and the evaluation of the frequency correlation function, in particular.

We have used *Mathematica* [15] to solve eqs. (22) - (25) numerically. In particular, we employed the ND solve function which iteratively and adaptively solves the equations to arbitrary accuracy (up to the working precision of the computer, of course) which we chose to be 10 digits in the final solution. The solutions for various initial conditions were calculated for varying lengths of time depending on the complexity of the trajectory. Thus, the results in Fig. 3 were obtained with 200 time units ($\hbar = c = 1$) while one of the Poincaré sections in Fig. 4 (see below) was obtained from a solution of length 10,000 time units (the longest of our trajectories).

As mentioned earlier, one measure of the accuracy of our solution is to compare the total energy E at the beginning and ending of each trajectory. For $E = -1.2661$ initially and the initial conditions stated above, we obtain $E = -1.2660$ after 10,000 time units.

Evaluating the numerical solutions to eqs. (22) - (25) at discrete time intervals, we find the frequency correlation function by discrete Fourier trans-

form, i.e. by replacing the integral in eq. (26) with a sum over the discrete time intervals of the trajectory. For our purposes it was sufficient to take the discrete time interval $\Delta t = 0.5$ which is more or less arbitrary. It is sufficient in the sense that the discrete nature of $\rho(\varphi, \varphi; \omega)$ is clearly evident, or not, depending on the particular value of the total energy and the initial conditions. Tests with smaller values of Δt on selected trajectories produced the same low frequency spectrum.

The length of the trajectories, τ, used to calculate $\rho(\varphi, \varphi; \omega)$ was also somewhat arbitrary. τ must be long enough to capture the basic low frequency structure. Again, our objective was to observe the qualitative behavior of the frequency correlation function rather than make a precise determination of its content, and we found that trajectories of length 200 time units were sufficient for this purpose. For the regular trajectories, increasing τ did not alter the frequency spectrum, and for the trajectories that exhibited chaotic character, increasing the trajectory length did not change the overall character of the frequency correlation function.

Finally, we note that $\rho(\varphi, \varphi; \omega)$ as calculated above is normalized to N times its continuum value, eq. (26), where $\tau = N\Delta t$.

To construct Poincaré sections, we simply evaluated each solution for a particular total energy at an arbitrary fixed value of one of the four variables while the others were allowed to vary. In practice, a small variation in the fixed d.o.f. was allowed to reduce the number of evaluations of the solution, i.e. our two-dimensional slice of phase space had a small but finite thickness. Also, to observe the characteristic phase space filling of the chaotic trajectories, τ was increased to as much as 10,000 time units.

Next, we present in Fig. 4 characteristic Poincaré sections for various higher energies. At $E = -12.44$ (initialized with $G = 0.01$) we still observe regular behavior, which is also obvious from the frequency correlation function (not shown). Notice that the trajectory is still completely confined to the right effective potential well, cf. Fig. 2, where it was initialized. Clearly, one expects that different initial conditions at the same energy would shift this Poincaré section w.r.t. the coordinate axes and distort it as well. At $E = -6.61$ the structure of the trajectories becomes much more complicated with the Poincaré section showing indications of break-up of KAM tori. This is better represented in the frequency correlation function, see. Fig. 5, where there are still outstanding discrete lines. However, they appear already considerably shifted w.r.t. to (integer multiples of) ω_0. Furthermore, there is

now a broad low-level background at fractional frequencies corresponding to the rather spiky character of the trajectory itself. From the Poincaré section it is obvious that the trajectory begins to run into the valley of the effective potential, cf. Fig. 2, which is the semiclassical equivalent to (attempts at) quantum mechanical tunneling to the other potential well ($\bar{\varphi} < 0$).

At $E = -1.266$ and $E = 15.6$ the Poincaré sections in Fig. 4 both show the "stochastic sea outlining islands of stability" which is the typical feature of irregular motion resulting from the break-up of KAM tori [1, 11]. Note that the lower energy here still corresponds to trajectories which classically could not get to the other side of the barrier at $\bar{\varphi} = 0$ (height $v(0) = 0$), i.e. they have to tunnel there. At $E = 15.6$ trajectories run well above the classical barrier and would yield regular motion in the classical limit. However, both cases show semiquantum chaos as a result of quantum corrections.

Finally, in Fig. 5 the frequency correlation function is also shown for two other energies, $E = -3.686$ and $E = 201.8$, which reveal further interesting features of our system. First, as expected, in the high energy limit the behavior becomes regular again, since the effective potential essentially becomes a single well with a perturbation of decreasing influence at the center. This is obvious from the appearance of the frequency correlation function. Presumably, its spectrum could be related to the quantum mechanical energy levels of the anharmonic $\bar{\varphi}^4$-oscillator relevant here at high excitation energy.

Secondly, and quite surprisingly indeed, we find at $E = -3.686$ regular behavior with a large number of discrete lines in the spectrum, which are rather evenly spaced and of comparable strength. It seems to originate from a resonance phenomenon leading to a fairly simple closed trajectory confined to one well, see Fig. 6. In distinction to the cases of Fig. 3, where the motion results from the quasi linear superposition of a few harmonic frequencies, at present the trajectory appears simple despite being fully nonlinear. This orderly behavior arises at an energy which lies in between cases with much more irregular if not fully chaotic trajectories, cf. Fig. 5. We did not yet investigate in full detail the sensitivity of this phenomenon to changes of the energy control parameter etc. In particular, it is an open question, whether other regular energy values like this one exist within the irregular intermediate energy regime. Preliminary investigations, however, show that this "resonating trajectory" is even sensitive to where precisely it is initiated on an equipotential contour, cf. Fig. 2. Presumably, we encounter a regime with stable KAM tori side by side with irregular domains [1, 11], which is

already indicated by the Poincaré sections in Fig. 4.

The results presented here naturally raise a number of more general questions. They will be discussed in the following section.

5 Conclusions

Presently, we have been studying semiquantum chaos in a simple one-dimensional double-well oscillator model. In the Introduction we explained the motivation for this and related studies by field theory considerations and nonrelativistic many-body problems [2, 4, 6, 8]. In this context our present work presents first steps towards a more detailed understanding of those more complicated systems and their behavior in the semiclassical regime, in particular.

Our work is based on the simple observation that a semiclassical description (employing the Gaussian variational principle or the TDHF approximation in our case, cf. Section III) necessarily involves the introduction of additional degrees of freedom beyond the classical ones, which may define the model. The corresponding additional coordinate and conjugate momentum variables are related to quantum fluctuations of the classical ones, i.e. they represent correlation functions of varying order (cf. below) in the quantum mechanical sense [3]. The classical and nonclassical degrees of freedom are governed by a coupled set of first-order autonomous differential equations, cf. eqs. (22) - (25). They are necessarily highly nonlinear, which to a major extent is the case independently of the particular dynamical model. Herein we find the potential for deterministic semiquantum chaos in this effective nondissipative Hamiltonian system.

Our numerical results presented in Section IV confirm the above considerations, in general. In Section III we argued that the total energy in our model, as determined, for example, by the parameters of the initial state wave function, cf. eq. (17), serves as the control parameter. Depending on the energy we find regular and chaotic trajectories as solutions of the semiclassical equations of motion. Besides Poincaré sections we mainly employed a suitably defined frequency correlation function, cf. eqs. (8), (26), which is related to the density matrix of the system to monitor its behavior. Here the transition to chaos could be expected to show up as a drowning of the discrete line structure deduced in Section II in a rising broadband noise. This was clearly observed in the numerical results, see, e.g., Fig. 5. However, quite

surprisingly we found that the behavior of the system as a function of the energy control parameter changes in a rather complex way. Apparently, regular and irregular regimes alternate with each other, where only the simplest cases (low/high energy limit) can be easily understood. The simple-minded stability analysis in Section III allows to outline qualitatively some regime of irregular behavior, but is quantitatively not sufficient to point out more of the detailed structure as a function of energy.

Clearly, our numerical studies show that there is room for more surprises in the behavior of the system depending on the control parameter. Furthermore, we did not fully explore the phase space of our system at a given energy: Are all initial conditions equivalent in that the corresponding trajectories are either regular or irregular? These problems, being intimately related to the question of ergodicity in the semiclassical model, can only be addressed through more extensive numerical work, which is beyond the scope of our present paper. Similarly, we did not investigate the nature of the transition to chaos in this system, nor did we look into details of the control parameter dependence of the frequency correlation function spectra.

However, our results together with the above considerations also point towards several issues of more general interest, which we discuss in the remaining part of this section.

It is convenient to introduce a formal representation of the exact wave function and Schrödinger equation for any quantum mechanical system which generalizes the Gaussian ansatz and variational equations of motion, eqs. (17) and (22) - (25), repectively. We rewrite the wave function,

$$\psi(x,t) = \exp f(x,t) \equiv \exp \sum_{n=0}^{\infty} f_n(t) x^n \quad . \tag{34}$$

This ansatz, of course, can only be considered as formal, since we do not know how to work out the normalization condition,

$$1 = \int dx\ \psi^* \psi = \int dx\ \exp\{2\mathrm{Re} f(x,t)\} \equiv F[\mathrm{Re} f_n(t)] \quad , \tag{35}$$

in general. Nevertheless, pretending we know the highly nonlinear functional F, we obtain a representation of the exact Schrödinger equation, cf. eq. (3), as an infinite autonomous set of coupled first-order differential equations,

$$i\dot{f}_0 \;\; = \;\; -\frac{2 \cdot 1}{2} f_2 + \frac{i}{2} \frac{\dot{F}}{F} \quad , \tag{36}$$

$$i\dot{f}_1 = -\frac{3\cdot 2}{2} f_3 + a \ , \tag{37}$$

$$i\dot{f}_2 = -\frac{4\cdot 3}{2} f_4 + b \ , \tag{38}$$

$$i\dot{f}_3 = -\frac{5\cdot 4}{2} f_5 + c \ , \tag{39}$$

$$i\dot{f}_4 = -\frac{6\cdot 5}{2} f_6 + d \ , \tag{40}$$

$$i\dot{f}_{n>4} = -\frac{(n+2)(n+1)}{2} f_{n+2} \ , \tag{41}$$

where we assumed for definiteness a simple polynomial potential, $v(x) = ax + bx^2 + cx^3 + dx^4$. Several observations seem worth mentioning here:

- The above exact representation of the full quantum dynamics is not limited to one dimension and can be extended to field theory using the functional Schrödinger picture, cf. [6, 7], for example. However, the power series ansatz, eq. (34), is not general enough or the most convenient one to cover all interesting cases and is used here only for heuristic reasons.

- There is an essential nonlinearity due to the normalization condition which, however, appears only in the first of the infinite set of coupled equations.

- Different polynomial type interactions enter the equations as different constant parameters only.

Based on these observations we conjecture the following. Any finite truncation of sufficiently high order ($n \leq N$) in such a nonlinear expansion scheme for the full quantum dynamics, even of a classically regular system, may lead to semiquantum chaos (in the sense presented in this paper) depending on the energy control parameter. In general, we expect additional classical conservation laws to lead to a higher dimensional control parameter space. Since the one and only non-linearity originates from the wave function normalization condition, cf. eqs. (35), (36), and enters the flow equations in a completely different manner than any interactions, we expect some still to be specified universality of the phenomena of semiquantum chaos.

Finally, knowing that any exact wave function solution of the linear Schrödinger equation cannot itself behave chaotically as discussed in Section

II, we are led to speculate that the infinite number of linearly coupled correlation degrees of freedom represented by eqs. (36) - (41) effectively restore the linear behavior of the full quantum dynamics. The latter here was only undermined by a single nonlinear constraint entering as a scale independent nonlinear coupling into one of the flow equations!

This brings us to the final topic of our discussion. In view of the linear character of the Schrödinger wave equation and particularly for classically regular systems one might be tempted to consider semiquantum chaos as a spurious effect caused by a truncation of the full quantum dynamics as described above or any other bad approximation thereof.

First of all, to illustrate the quality of the time-dependent Hartree-Fock approximation we include here Fig. 7 showing some typical comparisons between TDHF results and those of exact solutions of the Schrödinger equation for given initial conditions. Overall the expectation value of the position of the wave packet, for example, is always well described for sufficiently short times. Here the scale should be set by the characteristic time for the quantum mechanical spreading of the initial wave packet. Clearly, this has to depend on the energy at present. Even the long-time behavior is qualitively reproduced rather well in Fig. 7, no matter whether the TDHF trajectories are regular or chaotic at a particular energy. There is one notable exception here at $E = -1.266$, where TDHF for the chosen initial conditions is fully tunneling by a "roll-around" as discussed in Section II, whereas the major part of the exact wave packet stays is the initial well for long times. Obviously, TDHF misses some of the interference structure of full quantum mechanics. For further comparisons of TDHF and exact results in different quantum mechanical models we refer to Ref. [14].

In any case, however, one may argue that for a closed system the full quantum description is always better than any approximation. Thus, the way out of this apparent no-go situation, in order to establish the physical relevance of semiquantum chaos, is to allow for dissipative effects. Necessarily, one has to consider the interaction of the quantum system under study with its environment. In this way, the observation of semiquantum chaos is tied to the identification of suitable open quantum systems which through interactions with their decohering environment [16] are driven into the semiclassical regime.

Various steps in approaching a physically relevant dynamically enforced classical limit (not naively setting $\hbar \approx 0$) have been made [6, 12, 17, 18],

ranging in context from cosmology through strong interactions, questions of foundations of statistical mechanics, and the interpretation of quantum mechanics. Presently, with the examples discussed in the Introduction in mind, it seems most relevant to find systems, e.g. in solid state physics ("quantum dots" [19]), where environment-induced quantum decoherence and consequently semiquantum chaos become experimentally accessible.

Based on the example treated in Ref. [6], a quantum particle showing essentially classical behavior due to its interaction with a suitable quantized radiation field, the following model suggests itself for further study: the double-well oscillator governing a quantum particle coupled to a decohering radiation field. Before any detailed results, it would be interesting to see the effect of a deliberately chosen environment on the relevant set of flow equations, such as eqs. (36) - (41) above. We plan to address some of these fascinating problems in a future publication.

Acknowledgements: This work was supported in part by the University of Arizona (Tucson).

References

[1] H. G. Schuster, "Deterministic chaos: an introduction", 2nd ed. (VCH, New York/Weinheim 1989).

[2] F. Cooper, J. F. Dawson, D. Meredith and H. Shepard, Phys. Rev. Lett. 72 (1994) 1337.

[3] A. K. Pattanayak and W. C. Schieve, Phys. Rev. Lett. 72 (1994) 2855.

[4] G. Jona-Lasinio and C. Presilla, Phys. Rev. Lett. 68 (1992) 2269.

[5] L. H. Ryder, "Quantum Field Theory" (Cambridge University Press, Cambridge 1991).

[6] H.-Th. Elze, Nucl. Phys. B436 (1995) 213; Nucl. Phys. B (Proc. Suppl.) 39B,C (1995) 169; CERN-TH. 7297/94, hep-th/9406085.

[7] R. Jackiw and A. Kerman, Phys. Lett. 71A (1979) 158.

[8] E. J. Heller, J. Chem. Phys. 62 (1975) 1544.

[9] E. J. Heller and R. L. Sundberg, in "Chaotic Behavior in Quantum Systems", edited by G. Casati (Plenum Press, New York 1985), p. 255.

[10] P.A. Carruthers and F. Zachariasen, Rev. Mod. Phys. 55 (1983) 245.

[11] E. Ott, "Chaos in dynamical systems" (Cambridge University Press, Cambridge 1993).

[12] H.-Th. Elze, CERN-TH. 7372/94, hep-ph/9407377; in "Quantum Infrared Physics"; edited by H. M. Fried and B. Müller (World Scientific, Singapore 1995), p. 95.

[13] H. Grabert, P. Schramm and G.-L. Ingold, Phys. Rep. 168 (1988) 115.

[14] F. Cooper, S.-Y. Pi and P. N. Stancioff, Phys. Rev. D34 (1986) 3831.

[15] S. Wolfram, "Mathematica" (Addison Wesley, Reading MA 1991).

[16] W. H. Zurek, Phys. Today 44, No. 10 (1991) 36;
R. Omnès, Rev. Mod. Phys. 64 (1992) 339;
H. D. Zeh, Phys. Lett. A172 (1993) 189.

[17] W. H. Zurek and J. P. Paz, Phys. Rev. Lett. 72 (1994) 2508.

[18] M. Gell-Mann and J. B. Hartle, Phys. Rev. D47 (1993) 3345.

[19] M. A. Reed, Sci. American, Jan. 1993 (1993) 98.

Figure Captions:

Fig. 1: The double-well oscillator potential, eq. (2), with $\mu^2 = 1.0, \lambda = 0.06$. Also shown is a typical classical phase space trajectory ($\phi \equiv \bar{\varphi}$).

Fig. 2: The effective semiquantum potential, eq. (28), for $\phi \equiv \bar{\varphi} \geq 0$ (V is symmetric in ϕ). The inset shows the detailed shape of the contours close to the positive minimum (i.e. fixed point) of V.

Fig. 3: For two low energies (left/right column) the following TDHF results are shown (top to bottom): frequency correlation function, Poincaré sections in the two different coordinate/conjugate momentum planes, full trajectory (see text for details).

Fig. 4: Poincaré sections at various values of the energy (control parameter) illustrating the transition from regular to chaotic motion.

Fig. 5: Frequency correlation functions at various energies. Semiquantum chaos shows up as broadband noise in the expected line spectrum. There is an unexpected resonance effect at $E = -3.68601$.

Fig. 6: The nonlinear resonance trajectory discussed in the text.

Fig. 7: Comparisons between exact solutions of the time-dependent Schrödinger equation (full lines) and TDHF results (symbols) at various energies. Shown here is the expectation value of the position of the particle, which is initially a Gaussian wave packet.

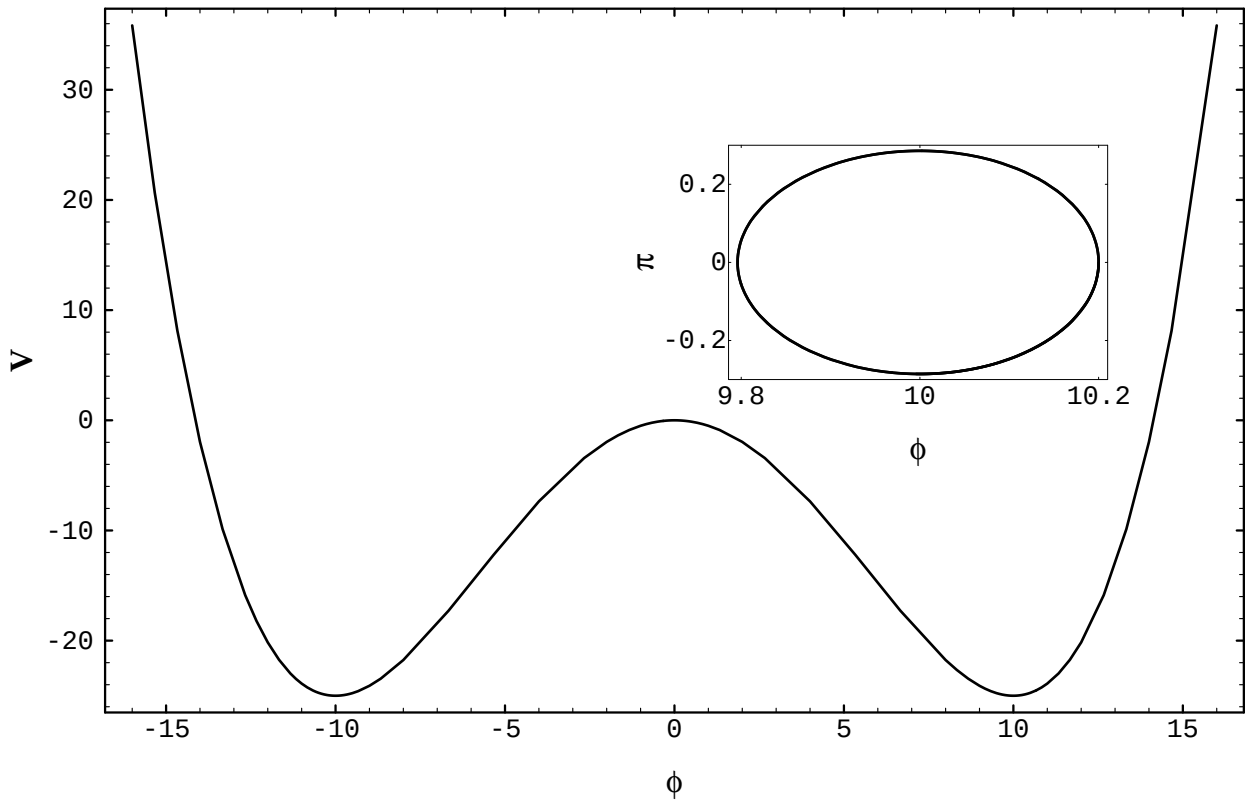
V
30
20
10
0
-10
-20
-15
-10
-5
0
5
10
15
ϕ
π
0.2
0
-0.2
9.8
10
10.2
ϕ

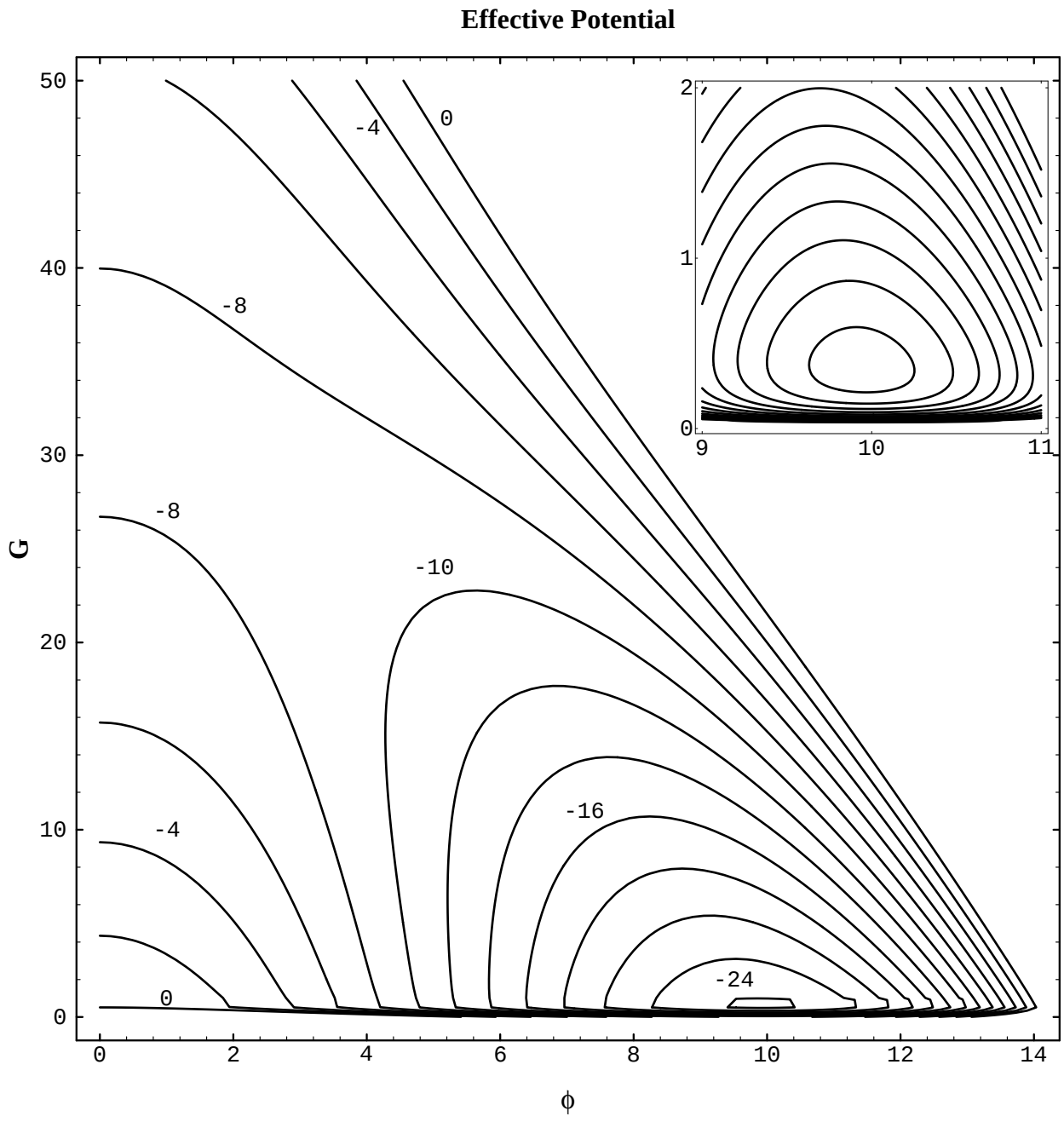
Effective Potential
G
ϕ
0
-4
-8
-10
-16
-24
0
2
4
6
8
10
12
14
0
10
20
30
40
50
9
10
11
0
1
2

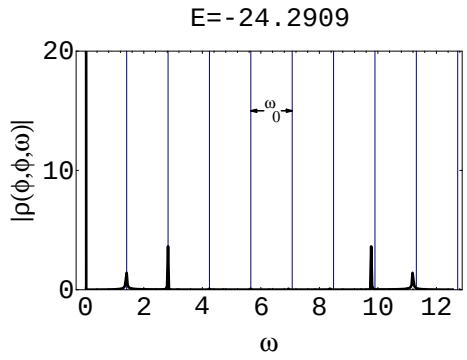
E=-24.2909
20
10
0
|ρ(ϕ,ϕ,ω)|
ω0
0 2 4 6 8 10 12
ω

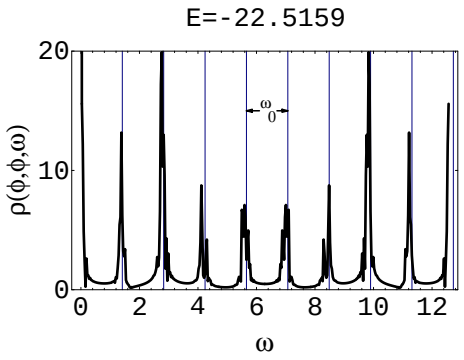
E=-22.5159
20
10
0
ρ(ϕ,ϕ,ω)
ω0
0 2 4 6 8 10 12
ω

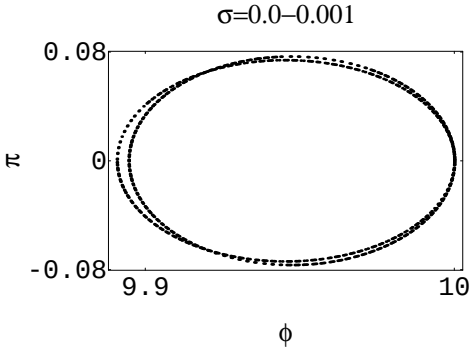
σ=0.0–0.001
0.08
0
-0.08
π
9.9
10
ϕ

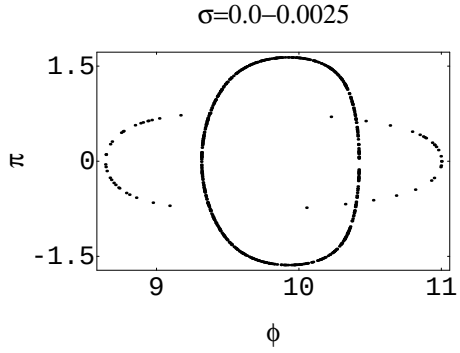
σ=0.0–0.0025
1.5
0
-1.5
π
9
10
11
ϕ

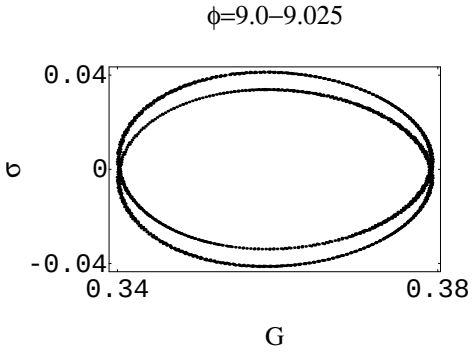
ϕ=9.0–9.025
0.04
0
-0.04
σ
0.34
0.38
G

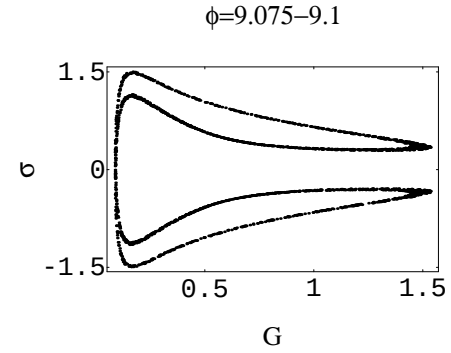
ϕ=9.075–9.1
1.5
0
-1.5
σ
0.5
1
1.5
G

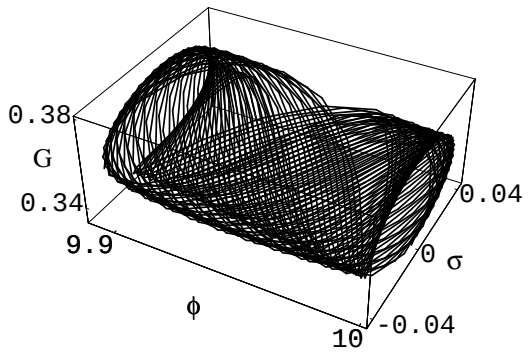
0.38
G
0.34
9.9
ϕ
10
0.04
0
σ
-0.04

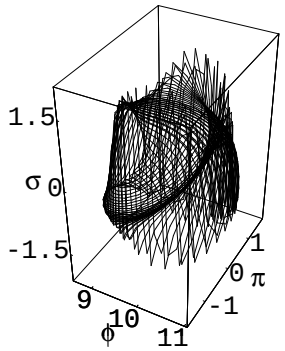
1.5
σ 0
-1.5
9
10
ϕ
11
1
0
π
-1

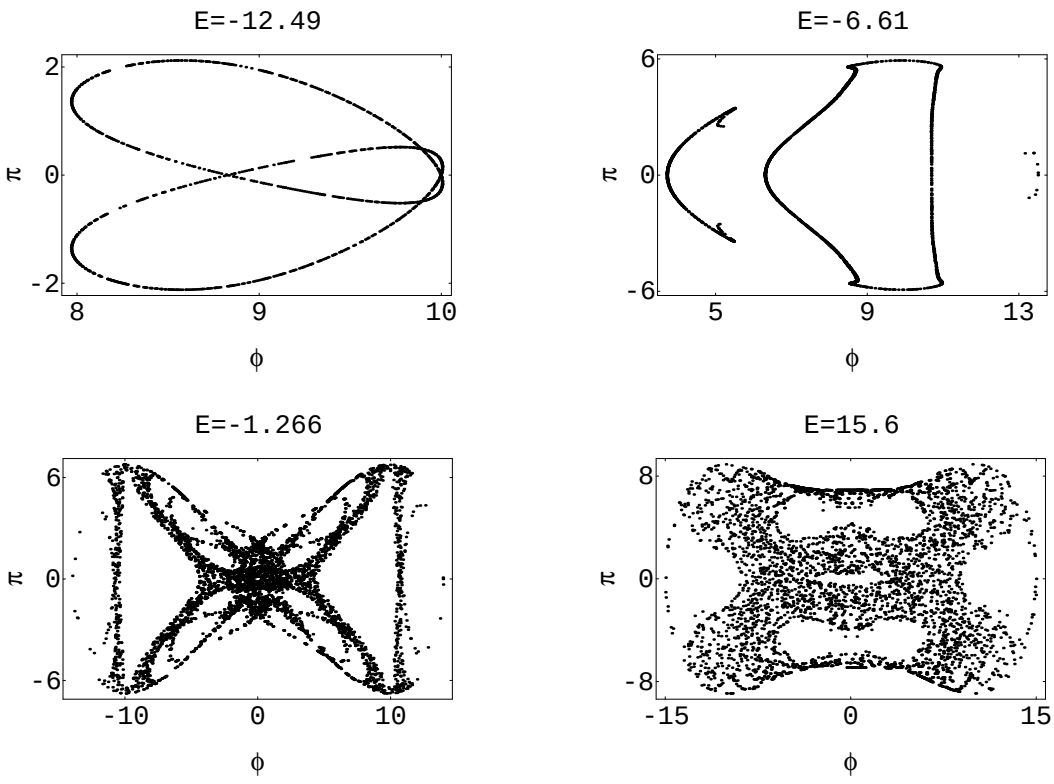
E=-12.49
E=-6.61
E=-1.266
E=15.6
π
ϕ
2
0
-2
8
9
10
6
-6
5
13
-10
-15
15

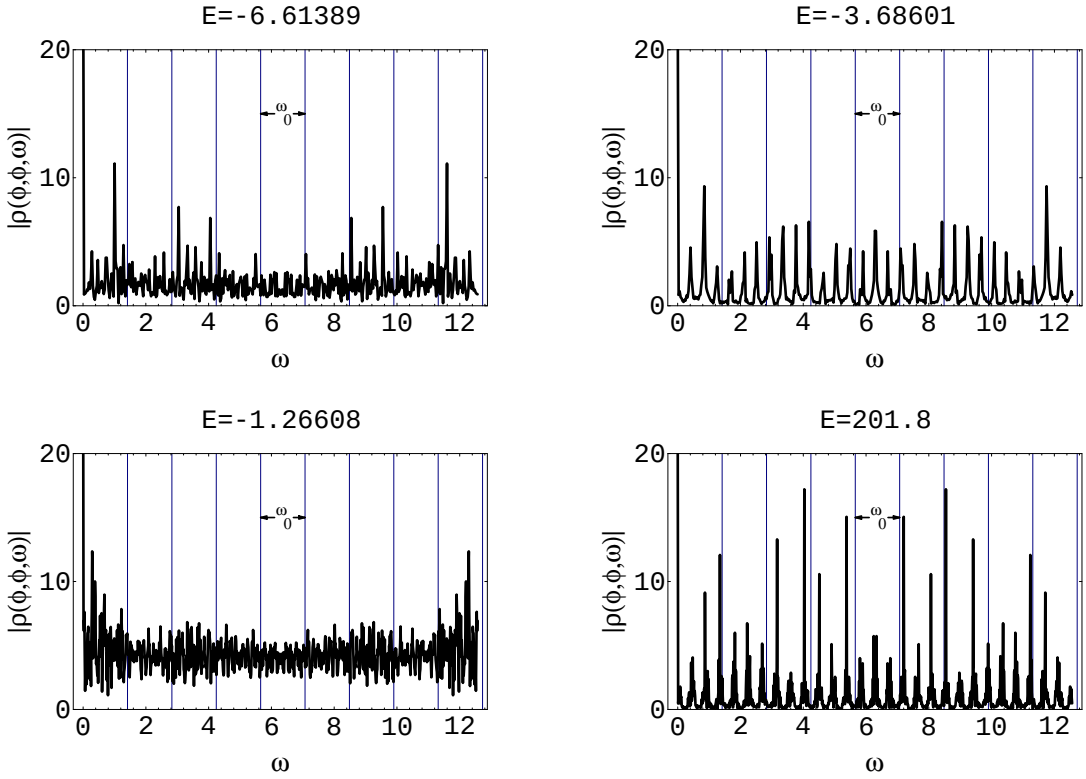
E=-6.61389
E=-3.68601
E=-1.26608
E=201.8
|ρ(ϕ,ϕ,ω)|
ω
ω0
0
10
20
0
2
4
6
8
10
12

E=-3.68601

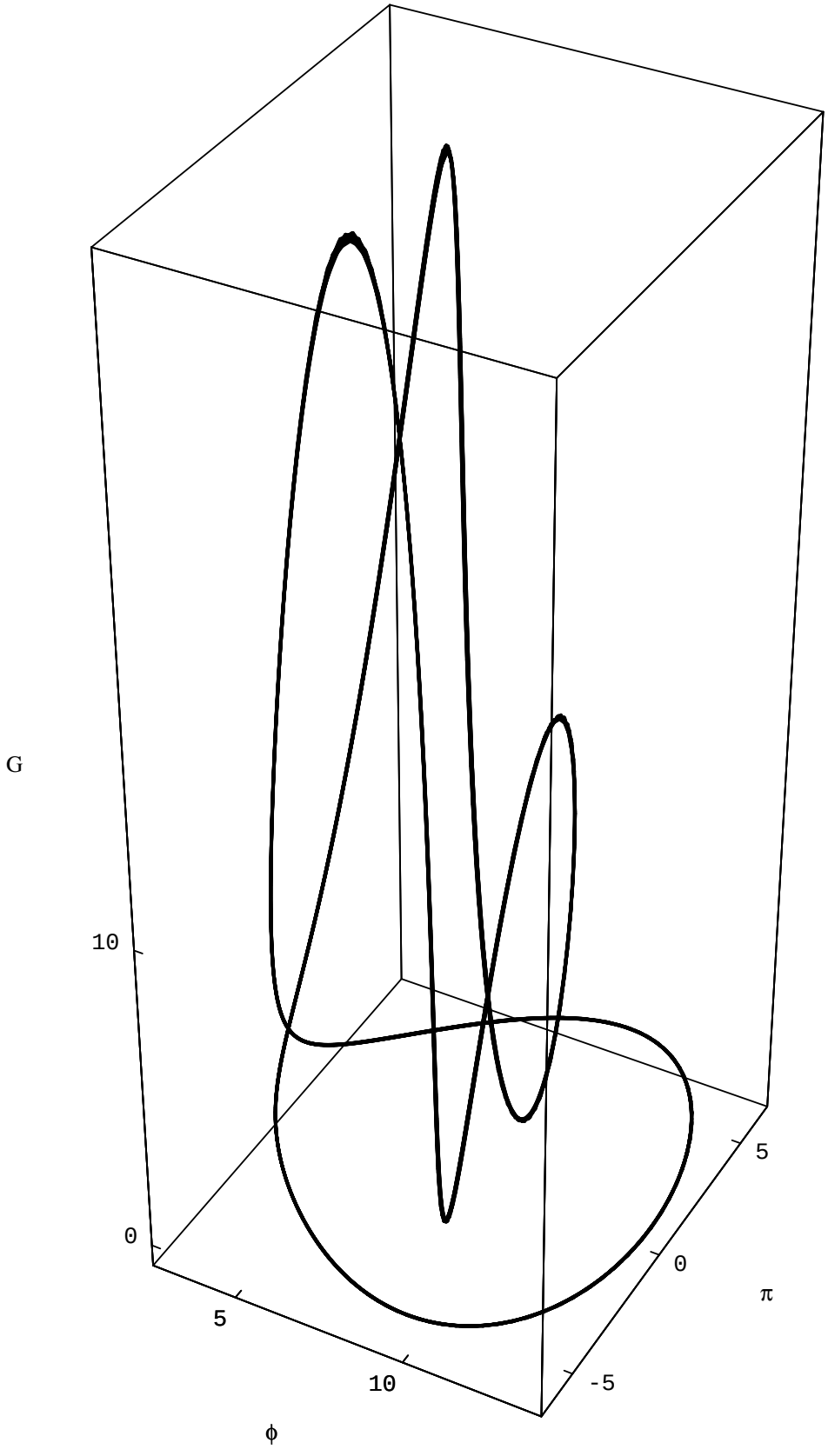

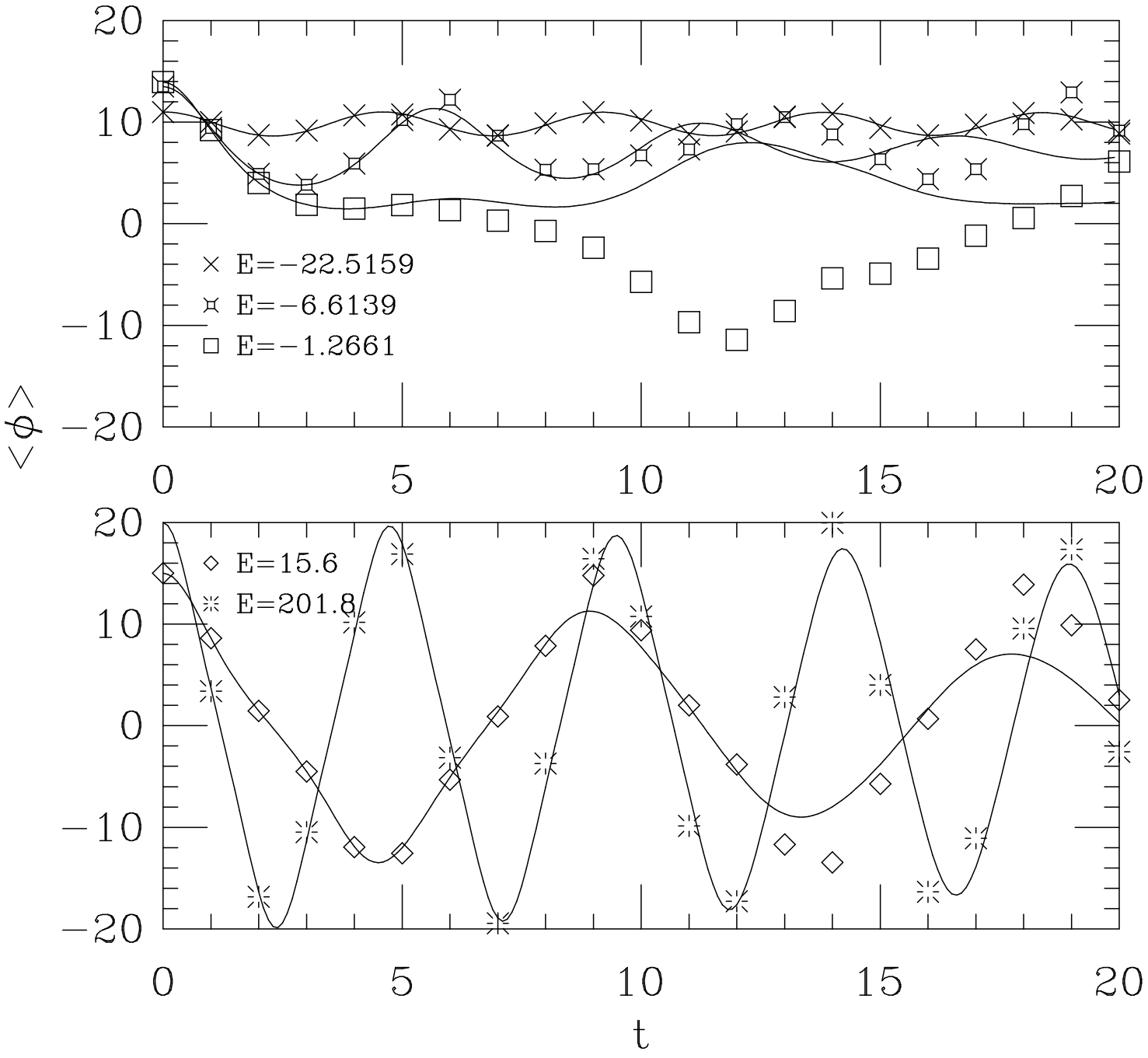
20
10
0
−10
−20
0
5
10
15
20
× E=−22.5159
E=−6.6139
E=−1.2661
E=15.6
E=201.8
< φ >
t